Ion mobility resolved photo-fragmentation to discriminate protomers

Chang Min Choi, Alexander Kulesza, Steven Daly, Luke Macaleese, Rodolphe Antoine, Philippe Dugourd, Fabien Chirot

Received: 30 April 2018 | Revised: 1 June 2018 | Accepted: 4 June 2018

DOI: 10.1002/rcm.8202

RESEARCH ARTICLE

WILEY Rapid Communications in Mass Spectrometry

Ion mobility resolved photo-fragmentation to discriminate protomers

Chang Min Choi[1] | Alexander Kulesza[2] | Steven Daly[2] | Luke MacAleese[2] | Rodolphe Antoine[2] | Philippe Dugourd[2] | Fabien Chirot[3]

[1] Mass Spectrometry and Advanced Instrumentation Research Group, Div. of Scientific Instrumentation, Korea Basic Science Institute, Cheongju, Republic of Korea

[2] CNRS, UMR5306 Institut Lumière Matière, Univ Lyon, Université Claude Bernard Lyon 1, 69622 Villeurbanne cedex, France

[3] CNRS, Ens de Lyon, UMR5280 Institut Sciences Analytiques, Univ Lyon, Université Claude Bernard Lyon 1, 69100 Villeurbanne, France

Correspondence
F. Chirot, Univ Lyon, Université Claude Bernard Lyon 1, CNRS, Ens de Lyon, UMR5280 Institut Sciences Analytiques, 69100 Villeurbanne, France.
Email: fabien.chirot@univ-lyon1.fr

Present address
S. Daly, Laboratoire ARNA, IECB-Université de Bordeaux, INSERM: U1212, CNRS: UMR5320, 2 rue Robert Escarpit, 33607 Pessac, France.

Funding information
FP7 Ideas: European Research Council, Grant/Award Number: 320659; Korea Basic Science Institute, Grant/Award Number: D38613

Rationale: Among the sources of structural diversity in biomolecular ions, the co-existence of protomers is particularly difficult to take into account, which in turn complicates structural interpretation of gas-phase data.

Methods: We investigated the sensitivity of gas-phase photo-fragmentation measurements and ion mobility spectrometry (IMS) to the protonation state of a model peptide derivatized with chromophores. Accessible interconversion pathways between the different identified conformers were probed by tandem ion mobility measurement. Furthermore, the excitation coupling between the chromophores has been probed through photo-fragmentation measurements on mobility-selected ions. All results were interpreted based on molecular dynamics simulations.

Results: We show that protonation can significantly affect the photo-fragmentation yields. Especially, conformers with very close collision cross sections (CCSs) may display dramatically different photo-fragmentation yields in relation with different protonation patterns.

Conclusions: We show that, even if precise structure assignment based on molecular modeling is in principle difficult for large biomolecular assemblies, the combination of photo-fragmentation and IMS can help to identify the signature of protomer co-existence for a population of biomolecular ions in the gas phase. Such spectroscopic data are particularly suitable to follow conformational changes.

1 | INTRODUCTION

The emergence of soft ionization techniques,[1-3] and then native mass spectrometry, has motivated the development of experimental strategies for the determination of the three-dimensional structures of molecular, and especially biomolecular systems in the gas phase. A wealth of techniques have been proposed as gas-phase structural probes, among which infrared multiphoton dissociation (IRMPD)[4-6] and ion mobility spectrometry (IMS)[7-18] have been the most widely used. The hierarchical structuration of biomolecules nevertheless renders the problem of structure determination particularly tricky to solve, thus justifying the combination of putatively complementary techniques. An appealing approach is to use a measure of the global shape of a molecule, like the collision cross sections measured by IMS, with more local information on the molecular arrangement that can be obtained from IRMPD, or other spectroscopic techniques.[19-32] Such attempts have nevertheless been limited to relatively small systems in general. Indeed, the expected complementarity is undermined on the one hand by the low structural sensitivity of IMS, and on the other hand by the increasing difficulty to interpret spectroscopic data (especially IR) as the size of the molecular system of interest grows.[32] Promising results have nevertheless been reported, which rely on energy transfer measurements between chromophores.[33-38] In particular, Förster resonance energy transfer (FRET) efficiencies could be determined for isolated ions, either through fluorescence[35] or fragmentation measurements,[33] and interpreted in terms of molecular distance. Moreover, the possibility to measure FRET on IMS-selected ions has recently been demonstrated.[39] An advantage of FRET against other spectroscopic techniques is that its interpretation does not rely on the assignment of spectral bands, and thus does not suffer from spectral congestion or prohibitive computational costs as

the number of atoms in the molecule increases. Indeed, FRET measurements on a full protein or on non-covalent complexes have been reported, illustrating the structural sensitivity of the technique, and its scalability to large biomolecular systems.[35,40,41]

One of the interests in performing structural studies on gas-phase ions is the possibility to precisely control the composition of the object under investigation through the selection of its mass-to-charge ratio, and possibly its IMS drift time. However, a particularity of gas-phase studies on multi-charged protonated (or deprotonated) ions is the possible ambiguity on the protonation sites. Different protonation patterns generally lead to differences in the gas-phase folding, which can often be separated by IMS. However, the attribution of the features observed in an IMS arrival time distribution to different conformers, resulting from the structural diversity of the systems, or to different tautomers is a complex task. Especially, the need to account for all possible combinations of protonation patterns can make molecular modeling simulations un-tractable.

In the present paper we examine the sensitivity of energy transfer measurements to different protonation patterns in a biomolecular system. The interplay between protonation and the optical and structural properties of small bio-molecular chromophores has already been investigated,[42] and we recently studied dye-tagged model peptides including different protonation patterns.[43] This contribution follows the same line by using a well-controllable model peptide, doubly tagged with a FRET donor-acceptor dye pair. The structural heterogeneities potentially present in such system comprise conformations, protonation pattern and the dye-tagging pattern. We present an experimental strategy to select single conformational families by ion mobility, in order to perform activation studies and photo-fragmentation measurements. The results are interpreted by systematic conformational landscape exploration with force-field-based molecular dynamics techniques and subsequent structural refinement using electronic structure calculations, after which we obtain energetic and ion-mobility-related predictions.

2 | EXPERIMENTAL

The peptide H-CA_2KA_2C-OH was purchased from GeneCust (Luxembourg) and was dissolved in H_2O to a concentration of about 1 mM. Carboxyrhodamine 575 C_5-maleimide (Setareh Biotech, Rh575) and QSY 7 C_5-maleimide (Life Technologies, QSY7) were used without further purification as donor and acceptor chromophores, respectively. Each chromophore was dissolved in dimethyl sulfoxide (DMSO) at a concentration of ~10 mM, and the peptide solution was mixed with Rh575 and QSY7 solutions to graft chromophores to the thiol groups of the peptide. Such grafting does not provide regioselectivity regarding the tagging sequence (i.e. Rh575-CA_2KA_2C-QSY7, Rh575-CA_2KA_2C-Rh575, QSY7-CA_2KA_2C-Rh575 and QSY7-CA_2KA_2C-QSY7 are present in the final solution). This final solution was diluted to a concentration of ~50 μM for the electrospray ionization.

The details of the experimental setup have been described elsewhere[44] and only a brief description is given below. All arrival time distributions (ATDs) were recorded using a tandem IMS instrument coupled to a high-resolution time-of-flight mass spectrometer. It allows selection of a particular isomer after a first drift tube (DT). The duration of the selection window is set to typically 500 μs, compatible with the time spread of the ion packet corresponding to a single isomer, due to diffusion. Selected ions can then be activated by collisions with buffer gas atoms before recording the ATD after the second DT.[43] Helium is used as a buffer gas at a pressure of 4 Torr, at the temperature of 300 K, and with typical voltage drops across first and second DTs of 400 V. Experimental collision cross sections (CCSs) are determined from the evolution of arrival times as a function of the inverse voltage across the second DT.[45] A quadrupole mass filter was then used for the selection of $[Rh575\text{-}CA_2KA_2C\text{-}QSY7]^{2+}$ and $[QSY7\text{-}CA_2KA_2C\text{-}Rh575]^{2+}$ (m/z 1039) after IMS separation. Photo-fragmentation measurements are performed by irradiation with a continuous wave laser (488 nm, 200 mW; Cobolt, Solna, Sweden) on mobility- and mass-selected ions stored in the collision cell of the instrument. The acceptor specific fragmentation yield was normalized to the intensity of the precursor ion without laser irradiation. The fragment ions at m/z 360 and 465 were previously identified as specific of QSY7 electronic excitation from a previous study.[33] The transmission efficiency for the ions at m/z 360 was too low in our IMS instrument so then only the peak at m/z 465 was used. To this end IM-MS spectra were accumulated for several thousand steps, alternating acquisitions with and without laser irradiation every 100 acquisition cycles.

3 | COMPUTATIONAL

Molecular dynamics simulations were performed with a parametrization already successfully used before for charged gas-phase peptides.[43,46] In brief, Amber99/GAFF parameters were used (with parameters for all considered protonation states of terminal chromophore-tagged cysteine residues re-evaluated as given in Kulesza et al[46]) employing the GROMACS molecular dynamics simulation software (version 5.1.3).[47-49] A velocity-verlet integrator with time step of 0.75 fs was employed. Temperature control was achieved by a velocity-rescaling algorithm (time-constant 1 ps). No bond-constraints and no nonbonded-interaction cutoffs were applied. Biased MD simulations (parallel-tempering well-tempered metadynamics simulations, PT-WTMetaD[50,51]) were performed using the PLUMED[52] code (version 2.3) plugged into GROMACS with the gyration radius[53] as order parameter. Structural and energetic refinement was done at the density functional theory (DFT) level employing the dispersion-corrected B97D functional for exchange and correlation[54] with an def2-SVP[55] basis set for the peptides consisting of 279 atoms. For these calculations, the Gaussian09 suite of software was used in Revision D.01.[56] Collisional cross sections were calculated using a local implementation of the trajectory method by Mesleh and coworkers.[57]

4 | RESULTS

4.1 | Ion mobility profile reveals multi-component gas-phase structural distribution

Figure 1a shows the full arrival time distribution (ATD) for m/z 1039, in the absence of mobility selection after DT1. Based on the peak

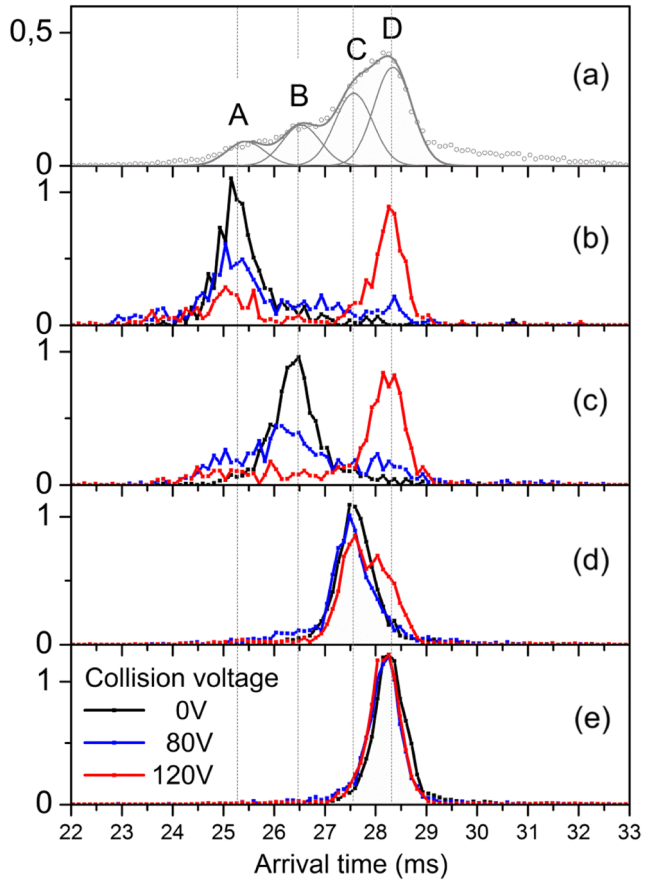

FIGURE 1 ATDs recorded for doubly charged ions at *m/z* 1039. Drift conditions: 4.0 Torr helium at 300 K, drift voltage: 400 V across 79 cm. (a) No IMS selection. The solid lines correspond to a Gaussian fit considering four components labelled A, B, C, and D. (b–e) ATDs recorded after IMS selection of each of the four populations, (black) without collisional activation, and with collisional activation using an accelerating voltage of (blue) 80 V and (red) 120 V

width expected from the resolution of the instrument, the present ATD cannot be attributed to a single conformational family of ions with identical cross sections. From a tentative fit using Gaussian functions of appropriate shape,[58] at least four different species co-exist. They are labelled from A to D respective to their increasing drift time. The corresponding experimental $^{exp}CCS_{He}$ values are listed in Table 1. The ATDs (plotted as black lines in Figures 1b, 1c and 1d) are recorded after selection of each of the above-mentioned species after separation in DT1. The blue and red lines show the changes in these ATDs when collisional activation is applied immediately after selection and before injection in DT2. Activation potentials ranging from 80 to 120 V are applied for each selected species. In the absence of activation, the observed ATDs all display a single peak, reflecting the selected time-window. This indicates that no spontaneous interconversion between the different structural families is detectable under the experimental conditions,[59-61] and further validates the identification of the above-proposed families.

TABLE 1 Experimental CCS values in helium at 300 K determined for the different species isolated from the ATD of ions at *m/z* 1039

Population	a	B	C	D
$^{exp}CCS_{He}$ (Å^2)	353	373	391	405

The uncertainty on the values is estimated to be 3%.

Upon collisional activation however, the different species display different behaviors. If peak A or B is selected, increasing activation energies result in a discrete shift of the ATD to larger drift times, ultimately tending to a single peak, similar to peak D. Note that activation of ions from peak B gives rise to the appearance of a small (possibly transient) population at the position of peak A. In contrast, no significant change is observed in the ATD when ions from peak D are selected and activated. Finally, the activation of peak C ions do show some change in their ATD, displaying a shoulder at a drift time corresponding to peak D. However, this effect is observed at activation voltages much higher than that necessary to induce transitions from A or B. Although it cannot be excluded that some transformation from peak C to peak D takes place (Figure 1d), it seems likely that the observed effect results from the small amounts of peak B ions present under peak C, due to their partial overlapping.

To summarize, according to results of the collisional activation, it seems peaks A, B, and D can interconvert. Following this scheme, the species in D presents some kind of final state that does not further react once a certain threshold of activation is applied. In contrast, the species contained in peak C do not seem to be connected to A, B or D through reactions that can be triggered by collisional activation. The latter statement can be further supported by the absence of significant population at the drift time of peak C when ions are activated from peaks A or B.

4.2 | Simulations suggests different protonation patterns being present

In order to determine which structural families of the peptide could contribute to the measured ion-mobility profile, we have performed a systematic structural exploration of the gas-phase structure with metadynamics simulations. The gyration radius of the molecules in well-tempered metadynamics with parallel tempering (PT-WTMetaD, see computational details) was used as a systematic exploration method, that accelerates high-barrier crossing and gives access to structural samples with a broad range of CCS values.[62] The method can tune from compact to unfolded configurations with a good chance that a configuration resembling the global minimum is sampled. With the knowledge of the stored biasing potentials of a converged simulation, an imprint of a free-energy profile (FEP) is accessible (in the formulation of WTMetaD, the accessible part of the FEP at a given temperature, to be more precise[51]). We have constructed all 12 combinations of dye-tagging (N-terminal Rh575 and C-terminal QSY7 and vice versa) and protonation patterns consistent with a 2+ charge state (see Table S1, supporting information). Convergence of the major features of the FEP (position and shape around the global free-energy minimum) of these relatively small systems was achieved after 2.5 ns of PT-WTMEtaD with two replicas). The FEPs with respect to the gyration radius for all 12 systems are given in Figure 2. Strikingly for such a peptide, where a multitude of conformations is expected to co-exist, only one global free-energy minimum well is obtained. The minimum is located in all cases at low gyration radii

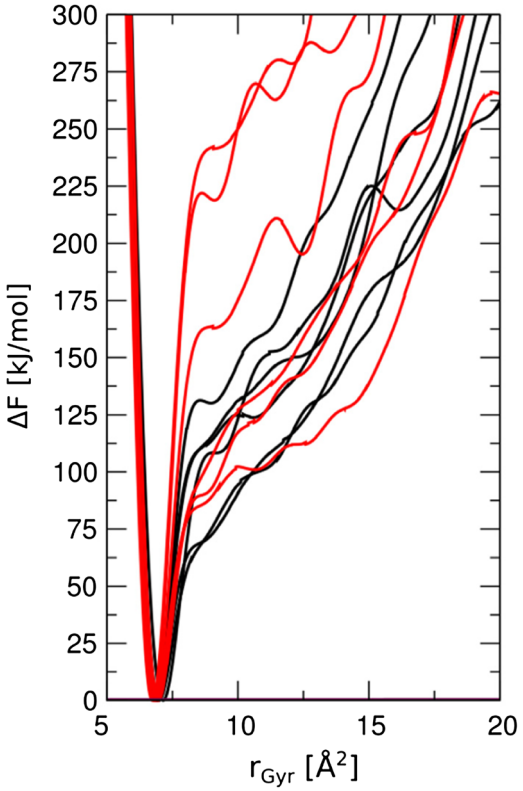

FIGURE 2 Results of Free-energy calculations. Free-energy profiles from analyzing metadynamics simulations with the gyration radius r_{gyr} as order parameter. Red and black curves correspond to the two grafting directions QRX and RQX, respectively, each assuming six different protonation patterns (see Table S1, supporting information)

(0.6–0.7 nm) indicating that the most compact structures are energetically preferred for each system. In contrast, no resolved minima are evidenced in the slightly higher r_{gyr} regime (0.7–1.0 nm) that would correspond to (meta) stable partially unfolded systems. This finding renders the presence of multiple conformational states for any of the possible protonation patterns unlikely.

Force-field energetics are not designed to accurately deduce relative energy differences of different protonation patterns. Therefore, the structural models were refined and their energetics estimated by DFT calculations starting from the lowest-energy structures (after force-field optimization of all collected metadynamics configurations). The final DFT energetics are listed in Table 2 and

TABLE 2 Main characteristics of the considered peptide topologies

Species	E_{DFT} [kJ/mol]	™CCS_{He} [Å^2]	R_{DA} [Å]	κ^2	E_{FRET}
RQ1	0	372	8.3	1.22	1.000
RQ2	33	381	13.5	0.49	0.998
RQ3	35	373	10.2	0.32	0.999
QR1	0	401	13.3	0.02	0.968
QR2	3	363	12.0	0.05	0.991
QR3	8	376	12.2	0.87	0.999

E_{DFT}: energy of the optimized structure at the DFT level relative to the lowest one for each sequence, ™CCS_{He}: CCS value computed using the trajectory method, R_{DA}: donor-acceptor separation, κ^2: orientational factor for FRET, E_{FRET}: theoretical FRET efficiency

Table S1 (supporting information) and Figure 3 together with a depiction of the final structural models. The properties of the three lowest-energy protonation states are considered (below 40 kJ/mol) which all have the titrable site of the rhodamine dye protonated (see Table S1, supporting information). It is interesting to note that it is not the charge-solvated but a zwitterionic type of structure that has a good chance to be the lowest in energy, a finding that is in line with earlier studies.[31,63] Upon explicit collision trajectory calculations, we can estimate the CCS for each structural prototype (predicted CCS values in Table 2).

The CCSs computed for the different conformers of $[Rh575\text{-}CA_2KA_2C\text{-}QSY7]^{2+}$, denoted RQ, all fall in a relatively narrow band centered around 375 Å^2. In contrast, the different protomers of the $[QSY7\text{-}CA_2KA_2C\text{-}Rh575]^{2+}$ sequence, denoted QR, possess a greater spread ranging from 363 to 401 Å^2. Comparison with the experimental CCS in Table 1 suggests that population A, with the lowest experimental CCS at 353 Å^2, is associated to the conformer with the lowest computed CCS: species QR2 with ™CCS_{He} = 363 Å^2. Following the same line, the ions from D ($^{exp}CCS_{He}$ = 405 Å^2) are associated with QR1 (™CCS_{He} = 401 Å^2). As peak B is found to interconvert to D upon collisional activation, it has to display the same grafting pattern as D. The population B may then be identified to QR3, the good agreement between the CCS further supporting the latter assignment. Moreover, the above assignations are also in line with the results of collisional activation experiments, since the most stable among the QR protomers, QR1, has been identified to population D, which appeared as the most stable configuration upon the interconverting populations.

In contrast to other populations, C ions were not found to interconvert to other peaks. This strongly suggests that C ions display a different grafting pattern. Indeed, the CCSs computed for all RQ protomers in Table 2 fall in a narrow CCS range compatible with the experimental CCS for C. Although RQ1 is found to correspond with the most stable species, the co-existence of different protomers with close CCS, difficult to resolve, is highly probable.

4.3 | Laser excitation indicates different excitation energy transfer characteristics within the IMS profile

Figure 4 shows the acceptor-specific fragmentation yield obtained from photo-excitation of ions from the different population identified for *m/z* 1039. Examples of associated mass spectra are given in Figures S1 and S2 (supporting information). Ions were stored in the collision cell of the instrument after mass and mobility selection. They were irradiated for 95 ms using a continuous wave laser at 488 nm. At this wavelength, only the rhodamine dye significantly absorbs light. Specific fragmentation of QSY7 then necessarily results from excitation coupling to rhodamine. The specific fragmentation yields shown in Figure 4 are then a measure of the strength of the coupling between electronic excitations in the two chromophores. Interestingly, the fragmentation yield significantly decreases as the CCS of the selected ion increases. Namely, population D has the highest CCS, and the lowest fragmentation yield, whereas A, with the lowest CCS, also displays the highest photo-fragmentation yield.

This could be qualitatively interpreted as an effect of the correlation between the compacity of the structure, and the proximity of the chromophores, leading to better coupling between the latter.

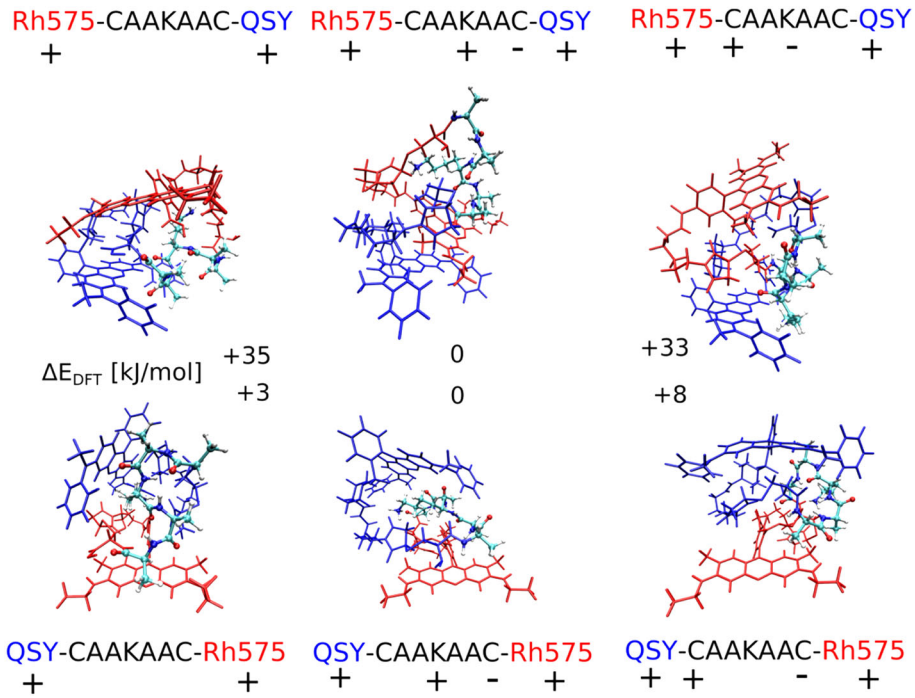

FIGURE 3 Structural representation of the energetically competent protomers (charge distribution depicted above and below structures) after DFT optimization. Rh575 is colored in red, QSY7 in blue. Relative DFT energies are also given. Results of CCS calculations for these species are given in Table 2

Such correlation was indeed previously reported in the case of FRET measurements.[33,39,64] In the case of FRET, the coupling efficiency between the chromophores depends in particular on the relative position of the chromophores, through their relative distance and orientation. The theoretical structural models (see Figure 3) were then analyzed in terms of the average chromophore separation (average distance, R_{DA}, between atoms contained in the xanthene-based optically active unit), and the orientational factor, κ^2, as defined in Kulesza et al.[46] The numerical results are listed in Table 2. With overall very close separations between 8 and 13 Å, FRET as model alone (mainly a statistical rate formulation and using dipolar electronic couplings) is usually regarded as inadequate to describe the full photo-physical mechanisms. Indeed, the FRET efficiencies that can be computed for the considered structures (Table 2) are all close to 1. In particular, exchange-coupling and orbital overlap type of interactions may lead to changes in energy transfer characteristics that (in the case of so-called Dexter transfer, referring to a situation driven by exchange coupling) has an exponential distance dependence. Such a short-distance energy transfer regime has recently been exploited through gas-phase photo-fragmentation experiments.[37] Moreover, fluorescence self-quenching has been shown to drastically increase photo-fragmentation yields when dyes are in close proximity.[34]

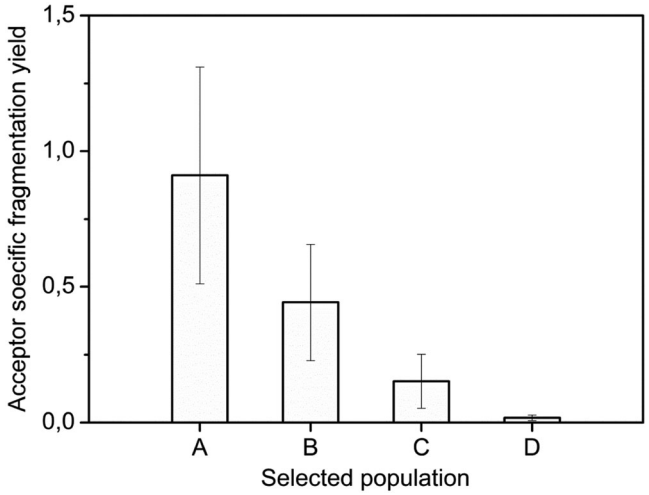

FIGURE 4 Acceptor-specific photo-fragmentation yields recorded for mobility-selected ions corresponding to the different populations (A–D) identified for doubly charged ions at *m/z* 1039 (see Figure 1). The error bars correspond to 95% confidence bands for the average yields

In the present case, no clear correlation could be found between the geometrical criteria for efficient FRET coupling, and the observed excitation coupling-related photo-fragmentation yields. Especially, the computed FRET efficiencies do not reflect the observed changes, and do not even follow the same trend. For example, the FRET efficiency computed for QR1 is far from being the highest among the considered models, even if it was attributed to population A, displaying the higher fragmentation yield.

5 | CONCLUSIONS

The present results show that the excitation coupling between chromophores in biomolecules can be strongly affected by the protonation pattern of the system. In particular, the unexpectedly large differences in inter-chromophore coupling measured for species with relatively close CCS values provide a clear signature that different tautomers are present. The origins of such differences nevertheless remain unclear, as no general trend can be drawn from experiments on a specific class of systems. The observed effect may be explained in

terms of perturbations of the optical properties of the chromophores by close-lying charged centers. In this case, both fluorescence-based and fragmentation-based measurements could be affected. Another reason why particularly low fragmentation yields are observed for certain tautomers might also be related to the possible presence of salt-bridges, preventing from actual detachment of the moieties after bond breaking. In the present case, the experimental observations from action-spectroscopy and IMS measurements could be interpreted with the help of molecular modelling. The computational cost of such an approach would naturally dramatically increase for heavier systems, like proteins. It is clear that no quantitative information can be extracted from the present photo-fragmentation measurements, especially in relation to the local structure of the investigated species. However, our results demonstrate that, even without a full understanding of the photophysics and relaxation dynamics in such systems, photo-fragmentation is highly sensitive to protonation sites, and can be useful to deconvolute IMS profiles by providing evidence for protomer coexistence. Furthermore, this sensitivity to protonation could be used to follow charge transfer or related conformational dynamics. This paves the way to dynamics measurements on gas-phase proteins in line with solution measurements.

ACKNOWLEDGEMENTS

This work was carried out with funding from the European Research Council under the European Union's Seventh Framework Program (FP7/2007-2013 Grant Agreement No. 320659). This work was supported by the research grant of the Korea Basic Science Institute (D38613).

ORCID

Chang Min Choi http://orcid.org/0000-0001-7708-9056
Rodolphe Antoine http://orcid.org/0000-0001-5682-8550
Fabien Chirot http://orcid.org/0000-0001-9115-9233

REFERENCES

1. Fenn JB, Mann M, Meng CK, Wong SF, Whitehouse CM. Electrospray ionization for mass spectrometry of large molecules. *Science*. 1989;246:64-71.
2. Fenn JB. Electrospray ionization mass spectrometry: How it all began. *J Biomol Tech*. 2002;13:101-118.
3. Aebersold R, Mann M. Mass spectrometry-based proteomics. *Nature*. 2003;422:198-207.
4. Polfer NC, Oomens J. Vibrational spectroscopy of bare and solvated ionic complexes of biological relevance. *Mass Spectrom Rev*. 2009;28:468-494.
5. Little DP, Speir JP, Senko MW, O'Connor PB, McLafferty FW. Infrared multiphoton dissociation of large multiply charged ions for biomolecule sequencing. *Anal Chem*. 1994;66:2809-2815.
6. Rijs AM, Oomens J. IR spectroscopic techniques to study isolated biomolecules. *Top Curr Chem*. 2014;364:1-42.
7. Ruotolo BT, Benesch JLP, Sandercock AM, Hyung S-J, Robinson CV. Ion mobility–mass spectrometry analysis of large protein complexes. *Nat Protoc*. 2008;3:1139-1152.
8. Konijnenberg A, Butterer A, Sobott F. Native ion mobility-mass spectrometry and related methods in structural biology. *Biochim Biophys Acta*. 2013;1834:1239-1256.
9. McLean JR, McLean JA, Wu Z, et al. Factors that influence helical preferences for singly charged gas-phase peptide ions: The effects of multiple potential charge-carrying sites. *J Phys Chem B*. 2010;114:809-816.
10. El-Baba TJ, Woodall DW, Raab SA, et al. Melting proteins: Evidence for multiple stable structures upon thermal denaturation of native ubiquitin from ion mobility spectrometry-mass spectrometry measurements. *J Am Chem Soc*. 2017;139:6306-6309.
11. Bohrer BC, Merenbloom SI, Koeniger SL, Hilderbrand AE, Clemmer DE. Biomolecule analysis by ion mobility spectrometry. *Annu Rev Anal Chem*. 2008;1:293-327.
12. Albrieux F, Calvo F, Chirot F, et al. Conformation of polyalanine and polyglycine dications in the gas phase: Insight from ion mobility spectrometry and replica-exchange molecular dynamics. *J Phys Chem A*. 2010;114:6888-6896.
13. Jurneczko E, Barran PE. How useful is ion mobility mass spectrometry for structural biology? The relationship between protein crystal structures and their collision cross sections in the gas phase. *Analyst*. 2011;136:20-28.
14. Wong RL, Williams ER, Counterman AE, Clemmer DE. Evaluation of ion mobility spectroscopy for determining charge-solvated versus salt-bridge structures of protonated trimers. *J Am Soc Mass Spectrom*. 2005;16:1009-1019.
15. Bernstein SL, Wyttenbach T, Baumketner A, et al. Amyloid β-protein: Monomer structure and early aggregation states of Aβ42 and its Pro 19 alloform. *J Am Chem Soc*. 2005;127:2075-2084.
16. Breaux GA, Jarrold MF. Probing helix formation in unsolvated peptides. *J Am Chem Soc*. 2003;125:10740-10747.
17. Lombardo CM, Collie GW, Pulka-Ziach K, et al. Anatomy of an oligourea six-helix bundle. *J Am Chem Soc*. 2016;138:10522-10530.
18. Uetrecht C, Barbu IM, Shoemaker GK, van Duijn E, Heck AJR. Interrogating viral capsid assembly with ion mobility–mass spectrometry. *Nat Chem*. 2011;3:126-132.
19. Masson A, Kamrath MZ, Perez MAS, et al. Infrared spectroscopy of mobility-selected H+–Gly-Pro-Gly-Gly (GPGG). *J Am Soc Mass Spectrom*. 2015;26:1444-1454.
20. Zucker S, Lee S, Webber N, Valentine S, Reilly J, Clemmer D. An ion mobility/ion trap/photodissociation instrument for characterization of ion structure. *J Am Soc Mass Spectrom*. 2011;22:1477-1485.
21. Poully JC, Lecomte F, Nieuwjaer N, et al. Combining ion mobility mass spectrometry and infrared multiphoton dissociation spectroscopy to probe the structure of gas-phase vancomycin–Ac2LKDADA non-covalent complex. *Int J Mass Spectrom*. 2010;297:28-35.
22. Lepere V, Le Barbu-Debus K, Clavaguéra C, et al. Chirality-dependent structuration of protonated or sodiated polyphenylalanines: IRMPD and ion mobility studies. *Phys Chem Chem Phys*. 2016;18:1807-1817.
23. Bellina B, Compagnon I, MacAleese L, et al. Binding motifs of silver in prion octarepeat model peptides: a joint ion mobility, IR and UV spectroscopies, and theoretical approach. *Phys Chem Chem Phys*. 2012;14:11433-11440.
24. Seo J, Hoffmann W, Warnke S, et al. An infrared spectroscopy approach to follow β-sheet formation in peptide amyloid assemblies. *Nat Chem*. 2017;9:39-44.
25. Fromherz R, Ganteför G, Shvartsburg AA. Isomer-resolved ion spectroscopy. *Phys Rev Lett*. 2002;89:083001.
26. Frankevich V, Martinez-Lozano Sinues P, Barylyuk K, Zenobi R. Ion mobility spectrometry coupled to laser-induced fluorescence. *Anal Chem*. 2013;85:39-43.
27. Hernandez O, Isenberg S, Steinmetz V, Glish GL, Maitre P. Probing mobility-selected saccharide isomers: Selective ion-molecule reactions and wavelength-specific IR activation. *J Phys Chem A*. 2015;119:6057.
28. Bellina B, Brown JM, Ujma J, et al. UV photodissociation of trapped ions following ion mobility separation in a Q-ToF mass spectrometer. *Analyst*. 2014;139:6057-6064.

29. Vonderach M, Ehrler OT, Matheis K, et al. Probing electrostatic interactions and structural changes in highly charged protein polyanions by conformer-selective photoelectron spectroscopy. *Phys Chem Chem Phys*. 2011;13:15554-15558.
30. Adamson BD, Coughlan NJA, Markworth PB, Continetti RE, Bieske EJ. An ion mobility mass spectrometer for investigating photoisomerization and photodissociation of molecular ions. *Rev Sci Instrum*. 2014;85:123109.
31. Drayss MK, Blunk D, Oomens J, et al. Gas-phase structures of solution-phase zwitterions: Charge solvation or salt bridge? *Int J Mass Spectrom*. 2009;281:97-100.
32. Le TN, Poully JC, Lecomte F, et al. Gas-phase structure of amyloid-β (12–28) peptide investigated by infrared spectroscopy, electron capture dissociation and ion mobility mass spectrometry. *J Am Soc Mass Spectrom*. 2013;24:1937-1949.
33. Daly S, Poussigue F, Simon A-L, et al. Action-FRET: Probing the molecular conformation of mass-selected gas-phase peptides with Förster resonance energy transfer detected by acceptor-specific fragmentation. *Anal Chem*. 2014;86:8798-8804.
34. Daly S, Choi CM, Chirot F, MacAleese L, Antoine R, Dugourd P. Action-self quenching: Dimer-induced fluorescence quenching of chromophores as a probe for biomolecular structure. *Anal Chem*. 2017;89:4604-4610.
35. Czar MF, Jockusch RA. Sensitive probes of protein structure and dynamics in well-controlled environments: combining mass spectrometry with fluorescence spectroscopy. *Curr Opin Struct Biol*. 2015;34:123-134.
36. Czar MF, Zosel F, König I, et al. Gas-phase FRET efficiency measurements to probe the conformation of mass-selected proteins. *Anal Chem*. 2015;87:7559-7565.
37. Hendricks NG, Lareau NM, Stow SM, McLean JA, Julian RR. Bond-specific dissociation following excitation energy transfer for distance constraint determination in the gas phase. *J Am Chem Soc*. 2014;136:13363-13370.
38. Hendricks NG, Julian RR. Two-step energy transfer enables use of phenylalanine in action-EET for distance constraint determination in gaseous biomolecules. *Chem Commun*. 2015;51:12720-12723.
39. Daly S, MacAleese L, Dugourd P, Chirot F. Combining structural probes in the gas phase – Ion mobility-resolved Action-FRET. *J Am Soc Mass Spectrom*. 2018;29:133-139.
40. Daly S, Knight G, Halim MA, et al. Action-FRET of a gaseous protein. *J Am Soc Mass Spectrom*. 2017;28:38-49.
41. Kulesza A, Daly S, Choi CM, et al. The structure of chromophore-grafted amyloid-β 12–28 dimers in the gas-phase: FRET-experiment guided modelling. *Phys Chem Chem Phys*. 2016;18:9061-9069.
42. Pedersen SØ, Byskov CS, Turecek F, Nielsen SB. Structures of protonated thymine and uracil and their monohydrated gas-phase ions from ultraviolet action spectroscopy and theory. *J Phys Chem A*. 2014;118:4256-4265.
43. Choi CM, Simon A-L, Chirot F, et al. Charge, color, and conformation: Spectroscopy on isomer-selected peptide ions. *J Phys Chem B*. 2016;120:709-714.
44. Simon A-L, Chirot F, Choi CM, et al. Tandem ion mobility spectrometry coupled to laser excitation. *Rev Sci Instrum*. 2015;86:094101.
45. Revercomb HE, Mason EA. Theory of plasma chromatography, Gazeous electrophoresis – Review. *Anal Chem*. 1975;47:970-983.
46. Kulesza A, Daly S, MacAleese L, Antoine R, Dugourd P. Structural exploration and Förster theory modeling for the interpretation of gas-phase FRET measurements: Chromophore-grafted amyloid-β peptides. *J Chem Phys*. 2015;143:025101.
47. Berendsen HJC, van der Spoel D, van Drunen R. GROMACS: A message-passing parallel molecular dynamics implementation. *Comput Phys Commun*. 1995;91:43-56.
48. Van der Spoel D, Lindahl E, Hess B, Groenhof G, Mark AE, Berendsen HJC. GROMACS: Fast, flexible and free. *J Comput Chem*. 2005;26:1701-1718.
49. Hess B, Kutzner C, van der Spoel D, Lindahl E. GROMACS 4: Algorithms for highly efficient, load-balanced, and scalable molecular simulation. *J Chem Theory Comput*. 2008;4:435-447.
50. Dama JF, Parrinello M, Voth GA. Well-tempered metadynamics converges asymptotically. *Phys Rev Lett*. 2014;112:240602.
51. Barducci A, Bussi G, Parrinello M. Well-tempered metadynamics: A smoothly converging and tunable free-energy method. *Phys Rev Lett*. 2008;100:020603.
52. Bonomi M, Branduardi D, Bussi G, et al. PLUMED: A portable plugin for free-energy calculations with molecular dynamics. *Comput Phys Commun*. 2009;180:1961-1972.
53. Vymětal J, Vondrášek J. Gyration- and inertia-tensor-based collective coordinates for metadynamics. Application on the conformational behavior of polyalanine peptides and Trp-cage folding. *J Phys Chem A*. 2011;115:11455-11465.
54. Grimme S. Semiempirical GGA-type density functional constructed with a long-range dispersion correction. *J Comput Chem*. 2006;27:1787-1799.
55. Weigend F, Ahlrichs R. Balanced basis sets of split valence, triple zeta valence and quadruple zeta valence quality for H to Rn: Design and assessment of accuracy. *Phys Chem Chem Phys*. 2005;7:3297-3305.
56. Frisch MJ, Trucks GW, Schlegel HB, et al. *Gaussian 09 Revision D.01*. Wallingford, CT: Gaussian Inc.; 2009.
57. Mesleh MF, Hunter JM, Shvartsburg AA, Schatz GC, Jarrold MF. Structural information from ion mobility measurements: Effects of the long-range potential. *J Phys Chem*. 1996;100:16082-16086.
58. Pierson NA, Chen L, Valentine SJ, Russell DH, Clemmer DE. Number of solution states of bradykinin from ion mobility and mass spectrometry measurements. *J Am Chem Soc*. 2011;133:13810-13813.
59. Pierson NA, Valentine SJ, Clemmer DE. Evidence for a quasi-equilibrium distribution of states for bradykinin $[M + 3H]^{3+}$ ions in the gas phase. *J Phys Chem B*. 2010;114:7777-7783.
60. Wyttenbach T, Pierson NA, Clemmer DE, Bowers MT. Ion mobility analysis of molecular dynamics. *Annu Rev Phys Chem*. 2014;65:175-196.
61. Poyer S, Comby-Zerbino C, Choi CM, et al. Conformational dynamics in ion mobility data. *Anal Chem*. 2017;89:4230-4237.
62. Calvo F, Chirot F, Albrieux F, et al. Statistical analysis of ion mobility spectrometry. II. adaptively biased methods and shape correlations. *J Am Soc Mass Spectrom*. 2012;23:1279-1288.
63. Jeanne Dit Fouque K, Lavanant H, Zirah S, et al. Gas-phase conformations of capistruin - comparison of lasso, branched-cyclic and linear topologies. *Rapid Commun Mass Spectrom*. 2015;29:1411-1419.
64. Daly S, Kulesza A, Poussigue F, et al. Conformational changes in amyloid-beta (12–28) alloforms studied using action-FRET, IMS and molecular dynamics simulations. *Chem Sci*. 2015;6:5040-5047.

SUPPORTING INFORMATION

Additional supporting information may be found online in the Supporting Information section at the end of the article.

How to cite this article: Choi CM, Kulesza A, Daly S, et al. Ion mobility resolved photo-fragmentation to discriminate protomers. *Rapid Commun Mass Spectrom*. 2019;33(S1):28–34. https://doi.org/10.1002/rcm.8202